Hindawi
International Journal of Antennas and Propagation
Volume 2024, Article ID 8777541, 8 pages
https://doi.org/10.1155/2024/8777541

Research Article

A Novel Ultra-Miniaturized Angularly Stable Frequency Selective Surface for L-Band Shielding Applications

Malathi Kanagasabai,[1] **Shini Ramadoss**,[1] **Lavanya Viswanathan**,[1] **Gulam Nabi Alsath Mohammed**,[1] **Shanmathi Shanmuganathan**,[1] **and Sandeep Kumar Palaniswamy**[2]

[1]*Department of Electronics and Communication Engineering, College of Engineering Guindy, Anna University, Guindy, Chennai 600025, Tamil Nadu, India*
[2]*SRM Institute of Science and Technology, Kattankulathur, Chennai, Tamil Nadu, India*

Correspondence should be addressed to Shini Ramadoss; shinyaboorva@gmail.com

Received 9 February 2023; Revised 10 January 2024; Accepted 27 January 2024; Published 7 February 2024

Academic Editor: Anna Pietrenko-Dabrowska

This paper presents a novel ultraminiaturized frequency selective surface (FSS) for L-band electromagnetic shielding applications. A basic square loop incorporated with folded arms in the top layer constructs the single-layer FSS design. Band-stop characteristics for the entire L-band operating frequency ranging from 1 GHz to 2 GHz are offered by the proposed design. An ultraminiaturized profile of $0.028\lambda o \times 0.028\lambda o$ is achieved by the designed FSS, where λo corresponds to the lowest operating frequency, achieving at least 32.1% miniaturization when compared to the state-of-the-art FSS designs in the literature. Polarization insensitivity with a peak shielding effectiveness of 45.4 dB is manifested by the rotational symmetry of the proposed design. The proposed FSS exhibits excellent angular stability performance up to 80° with a frequency deviation of less than 1%. The equivalent circuit model helps to understand the working principle of the proposed FSS. The experimental results of the designed FSS prototype agree well with the simulation results. Hence, the proposed spatial filter is a suitable candidate for enhancing security in wireless communication at the carrier frequencies of GPS systems.

1. Introduction

Electromagnetic interference (EMI) causes impairment in wireless devices when it is exposed to hazardous electromagnetic waves [1]. Conventional metallic shields are utilized to completely block all the frequencies of incoming electromagnetic waves. The advent of frequency selective surface is an alternate approach to mitigate the effect against EMI due to its band-stop characteristics. The spatial filter offers selective performance on a particular frequency for its geometric nature. Frequency selective surfaces have tremendous growth for the applications of reflectors [2, 3], spatial filters [4], and shielding applications [5, 6]. Frequency selective surfaces act as an EMI shielding for the communication devices which increases the security in satellite and military applications. Nowadays, the increasing demand for frequency selective surfaces is the miniaturized footprint, simpler geometry with high angular stability, high shielding effectiveness, and stable polarization performances.

The large-sized FSS screen will produce a grating region closer to the operating band which tends to affect the frequency selectivity characteristics of the FSS [7]. The miniaturization configuration is a quintessential feature due to its finite size realization in limited space occupancy for real-time applications [8]. To achieve a miniaturized profile, 2.5D design approach is used in FSS with a multilayer structure incorporating conductive holes which leads to a complex bulkier structure reported in [9]. Designing a compact FSS with a 2D single-layer structure without using vias is a challenging task. Thus, the frequency selective surface with the aforementioned prominent features is designed with a miniaturized configuration with a single-layer structure

that exhibits band-stop characteristics which are considered advantageous features for security purposes in wireless communication systems.

Recently, several novel design approaches for the miniaturized FSS unit cells are discussed in [7–17]. Meandering lines connected with conductive holes are embedded on a triple-layer substrate to achieve the miniaturized FSS depicted in [8] which achieves angular stability up to 60 degrees. Even though the FSS unit cell with multiple layers provides a higher impedance bandwidth, it increases the FSS thickness and makes the design complex which leads to fabrication costlier. Subsequently, the research works are performed on a single-layer miniaturization. A meandered peak [7], Hilbert fractal loop [10], and Jerusalem cross loop [11] are used to design a band-stop FSS unit cell. All the abovementioned FSS unit cells [7, 8, 10, 11] are not considered small-scale dimensions.

The FSS unit cell proposed in [9] uses a fractal four-legged loaded loop, tapered convoluted stripe [12], and square loop knitted structure [13] to block the incoming EM wave. In addition, the FSS in [9, 12, 13] uses both the top and bottom layers connected using the conductive holes. The miniaturized FSS in [14] having the handshake convoluted loop and a complex design composed of zig-zag inductive arms [15] is proposed. In the aforementioned work [14, 15], angular stability is achieved only up to 60°. In [16], an asymmetric convoluted miniaturized FSS is depicted which makes the FSS unit cell polarization dependent on various angles of phi. An active miniaturized FSS unit cell is designed using metallic parallel plates in [17]. However, the significant issue in the use of active components is the fabrication cost and additional voltage supply. The miniaturized FSS exhibits dual-band response for stealth applications which is mentioned in [18] and the wideband concentric ring frequency selective surface for 5G devices is discussed in [19]. The generalized idea about designing FSS is explained in [20–22]. The FSS with a large unit cell size exhibiting band-stop characteristics is given in [23]. The FSS unit cells given in [24–28] were designed using a complex design using a multi-layer configuration, which is not a cost-effective solution.

To overcome the limitations of the literature survey, this paper demonstrates a single-layer miniaturized band-stop FSS for shielding the entire L-band. The miniaturized profile of the proposed FSS unit cell is $0.028\ \lambda o \times 0.028\ \lambda o$, for the lowest operating frequency at 1 GHz. The proposed FSS unit cell is 32.1% smaller when compared to existing art of work [7] without adding conductive holes. In addition, the proposed FSS unit cell flaunts angular stability up to 80° with a peak shielding effectiveness of 45.4 dB and polarization insensitivity of up to 90° for both TE Mode and TM Mode. This FSS acts as a shield for the entire L-band signal from 1 GHz to 2 GHz, as the L-bands are the carrier frequencies for satellite navigation (GPS). In this letter, the section is summarized as follows: the topology of the FSS unit cell with its equivalent circuit model analysis is demonstrated in Section 2. The experimental validation of the fabricated prototype with its measurement setup is illustrated in Section 3. Finally, the conclusion followed by reference is presented in Section 4.

2. Design of FSS Unit Cell

2.1. Topology of FSS Unit Cell. The 2D FSS unit cell having a single layer and its side view is depicted in Figures 1(a) and 1(b), respectively. The FSS was constructed using a 1.6 mm thick (h) FR-4 substrate having a permittivity of 4.3 and a loss tangent of 0.025. The size of the FSS is designed with a thickness of only 0.0054 λo, making it suitable for compact systems. The top layer encompasses a square-centered PEC patch extended with rectangular and L-stub having a thickness of 0.035 mm. The periodicity of the proposed FSS unit cell is 8.4 mm along the x and y directions. The simulation is carried out in CST Microwave Studio (2018). The unit cell design starts with the basic square loop structure. The convoluted technique is incorporated in the unit cell design to increment the electrical length to achieve the lowest operating frequency. The proposed FSS design is based on four-fold rotational symmetry to exhibit polarization insensitivity performance.

2.2. Evolution of the FSS Unit Cell. The evolution of the proposed FSS unit cell with its transmission coefficient response is depicted in Figure 2. The simulation is carried out in CST Microwave Studio (2018). The proposed FSS unit cell initiates with the basic square loop of length 2.4 mm in Stage 1. The square loop resonates from 18.59 to 19.82 GHz with a bandwidth of 1230 MHz. In Stage 2, a rectangular stub of area 1.31 mm^2 is connected to the square loop with a meandering line of length 1.76 mm. It produces a bandwidth of 1580 MHz resonating from 11.907 GHz to 13.487 GHz. The area of the rectangular stub is increased to 3.31 mm^2 with a meandering line of 2.4 mm to achieve the frequency range from 7.1 GHz to 7.9 GHz in Stage 3. To enhance the bandwidth and lower the frequency range in Stage 4, an L-Stub is incorporated to increase the electrical length, thus providing the lowest operating frequency of 1 GHz and achieving the peak shielding effectiveness of 45.4 dB for the frequency range from 1 GHz to 2 GHz.

2.3. Surface Current Distribution. Surface Current assists in understanding the relationship between the operating frequency and length of the resonating arms. The vertical and horizontal flow of the surface current in TE and TM Mode is observed in Figures 3(a) and 3(b) around the resonating arms. Thus, the length (L) for the proposed FSS unit cell is calculated as follows:

$$\mathrm{L} = 2 * (\mathrm{L1} + \mathrm{L2} + \mathrm{L3} + \mathrm{L4} + \mathrm{L5} + \mathrm{L6} + \mathrm{L7}), \qquad (1)$$

$L = 41.2752$ mm, corresponds to the quarter wavelength ($\lambda/4$) opertating frequency as, $f_r = c/4 * \mathrm{L} * \sqrt{(\varepsilon_r + 1)/2}$ (1), where$\varepsilon_r$is the dielectricconstant of the substrate. From

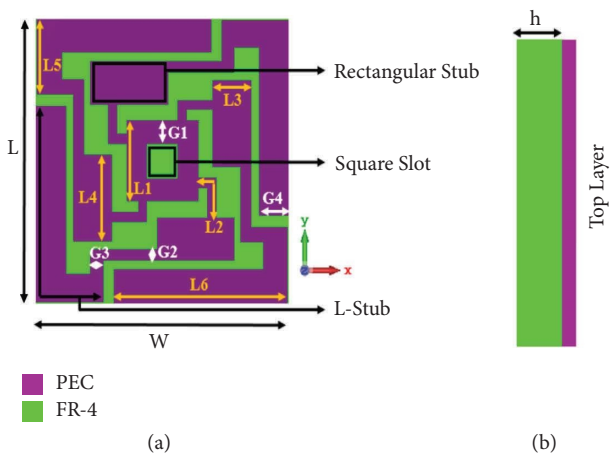

Figure 1: (a) Proposed 2D FSS unit cell in front view with material specifications. Geometric specifications with labels of the proposed FSS unit cell: L = W = 8.4 mm, L1 = 2.4 mm, L2 = 1.76 mm, L3 = 1.29 mm, L4 = 2.57 mm, L5 = 2.24 mm, L6 = 5.79 mm, G1 = 1.38 mm, G2 = 0.3 mm, G3 = 0.7 mm, and G4 = 0.99 mm. (b) Side view.

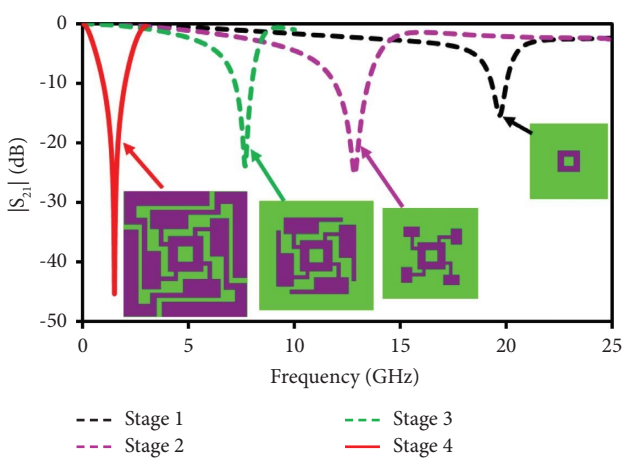

Figure 2: Simulated transmission coefficient characteristics of the proposed FSS unit cell at each evolution stage.

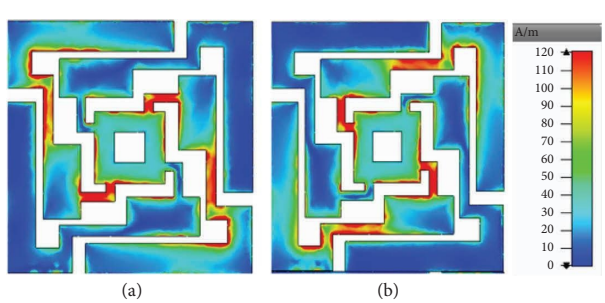

Figure 3: Surface current distribution at 1 GHz. (a) TE mode. (b) TM mode.

equation (1), the operating frequency (f_r) obtained is 1.123 GHz, which approximated the resonating frequency of 1 GHz. Thus, the FSS unit cell for the desired operating frequency is proposed by varying the surface current path length.

2.4. Equivalent Circuit Modeling. The theoretical interpretation is understood by the implementation of an equivalent circuit for the proposed FSS unit cell. The equivalent circuit for the proposed FSS unit cell highly depends on the geometry and surface current. Thus, the strong current density flowing in the same direction is indicated with a lumped inductor and capacitor in a series combination as shown in Figure 4(a). The mutual coupling plays a significant role in occurring due to the presence of displacement current produced between the metal patch. The resonator arms act as a lumped inductor L_1 with the mutual coupling between the arms playing the role of capacitance (C_1) as depicted in Figure 4(a). The effect between the patch in the FSS unit cell is insignificant and therefore, the mutual inductance is eliminated. The mutual coupling between the adjacent unit cells as depicted in Figure 4(b) is indicated by the capacitor C_{coup}. The resonant poles are produced by the addition of a capacitor C_{coup} with a conventional series LC circuit. Thus, the band-stop behavior for the entire L-band is achieved accurately. The impedance of the circuit for a series inductor (L_1) and capacitor (C_1) shown in Figure 4(c) is mathematically expressed as follows:

$$Z_s = j\omega L_1 + \frac{1}{j\omega c_1}. \tag{2}$$

The total impedance (Z) by the addition of coupling capacitance is given by the following equation:

$$Z = Z_s \left\| \left(\frac{1}{j\omega C_{coup}} \right) \right. . \tag{3}$$

By equation (3), we get the following equation:

$$Z = \frac{\left(1 - \omega^2 L_1 C_1 / \omega^2 c_1 C_{coup}\right)}{\left(C_{coup} - \omega_1^2 L_1 c_1 C_{coup} + c_1 / j\omega_1 c_1 C_{coup}\right)}. \tag{4}$$

The frequency for the proposed FSS unit cell is obtained by equating the poles and zeros to 0.

From equation (4), we get the following equation:

$$\omega^2 = \frac{1}{L_1 C_1} \text{ and } \omega_1^2 = \frac{C_1 + C_{coup}}{L_1 C_1 C_{coup}}. \tag{5}$$

Assuming L_1 is known, the values of C_1 and C_{coup} are determined from equation (5). C_{coup} contributes to the bandwidth for the required frequency range from 1 GHz to 2 GHz. The transmission zero is given by ω_1, and ω represents the transmission poles in equations (6) and (7).

$$C_1 = \frac{1}{\omega^2 L_1}, \tag{6}$$

$$C_{coup} = \frac{C_1}{\left(\omega_1^2 / \omega^2\right) - 1}. \tag{7}$$

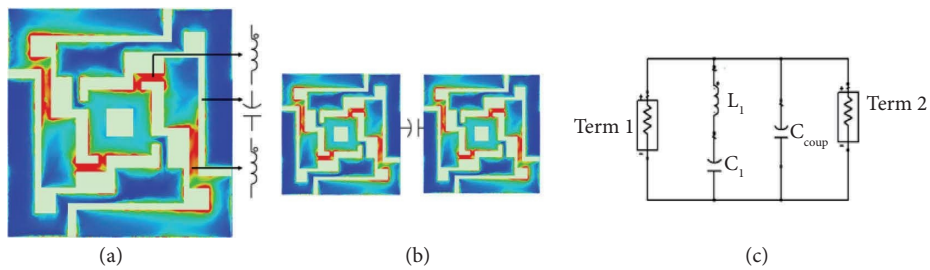

Figure 4: (a) Front view of the proposed FSS in TE mode with electrical circuit components. (b) Effect of the lumped component with adjacent FSS unit cell. (c) Equivalent circuit model for the proposed FSS unit cell.

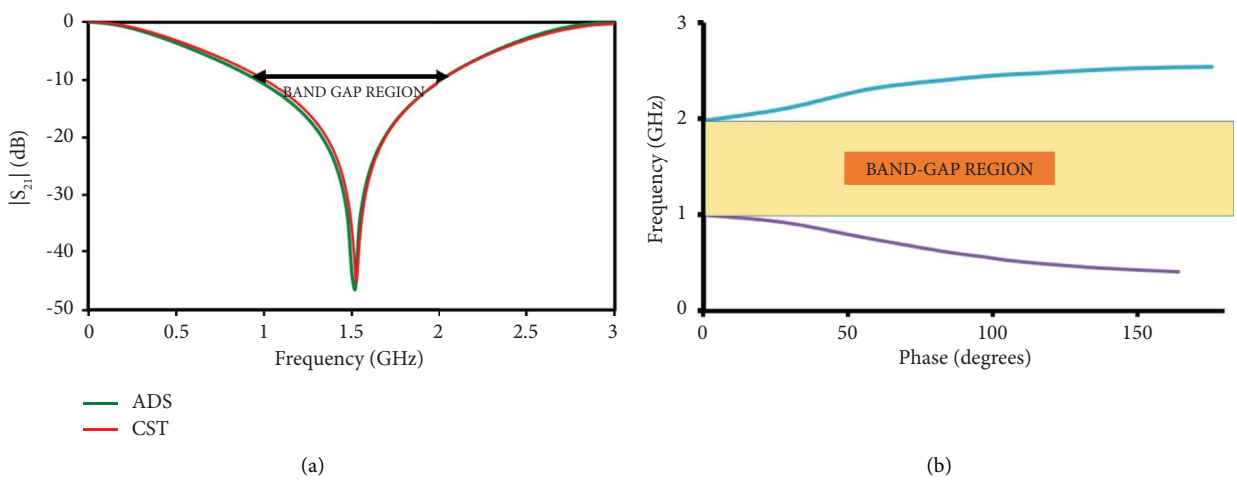

Figure 5: (a) Transmission coefficient analyzed in CST and ADS. (b) The dispersion curve of the proposed FSS model.

The inductor L_1 is determined by the iterative procedure with the help of tuning in ADS software. The values for the proposed equivalent circuit in Figure 4(c) are calculated as $L_1 = 1.12$ nH, C9.9pF, and $C_{coup} = 3.3$ pF. The transmission response is computed in ADS for the proposed equivalent circuit. The behavior of the proposed FSS unit cell is verified by comparing the transmission characteristics of CST and ADS as depicted in Figure 5(a). It is evident that the proposed equivalent circuit exhibits the band-stop response from 1 GHz to 2 GHz. To verify, the operating frequency can also be analyzed by the following equation:

$$f = \frac{1}{2\pi\left(\sqrt{\left(C_1 + C_{coup}\right)L_1}\right)}. \quad (8)$$

The dispersion diagram is incorporated to analyze the functioning of the FSS. The Bloch wave vector has a region where no Eigen frequencies have been discovered, indicating that electromagnetic fields are not allowed in that frequency range. This region is known as the band gap. The band-gap region of the proposed FSS is analyzed by adopting a dispersion diagram depicted in Figure 5(b). The dispersion diagram is validated by using the Eigen mode solver in CST Microwave Studio. The dispersion curve for the desired modes is selected through the Eigenmode solver which provides information about the band-stop operation of the proposed FSS. The dispersion curve in Figure 5(b) shows that the existence of a wide band gap between two propagating bands ensures that no modes of propagation are allowed to be transmitted. This region will be claimed as a band-stop region for the proposed FSS. Therefore, a band-stop response is obtained in the frequency region from 1 GHz to 2 GHz, where the electromagnetic waves cannot propagate through the proposed FSS.

2.5. Parametric Analysis. The influence of the width of meandering lines has a great impact on the bandwidth of the proposed FSS unit cell as depicted in Figure 6(a). The parameter G4 is varied to analyze the operating frequency range from 1 GHz to 2 GHz. The width of the resonating arms decreases from 0.99 to 0.69 which reduces the operating frequency to 0.8–1.8 GHz. In Figure 6(b), the length of L6 is increased from 1.93 mm to 5.79 mm which results in reducing the operating frequency from the higher frequency band (7.1–8.1 GHz) to the lower frequency band (1-2 GHz). From Figures 6(a) and 6(b), it is inferred that the length (L6) is inversely proportional, and the width (G4) is directly proportional to the operating frequency. The operating frequency decreases with an increase in length and a decrease in the width of the resonator. Hence, the length and width of the resonating arms are compromised to achieve the required operating range in a single-layer miniaturized surface for L-band shielding applications.

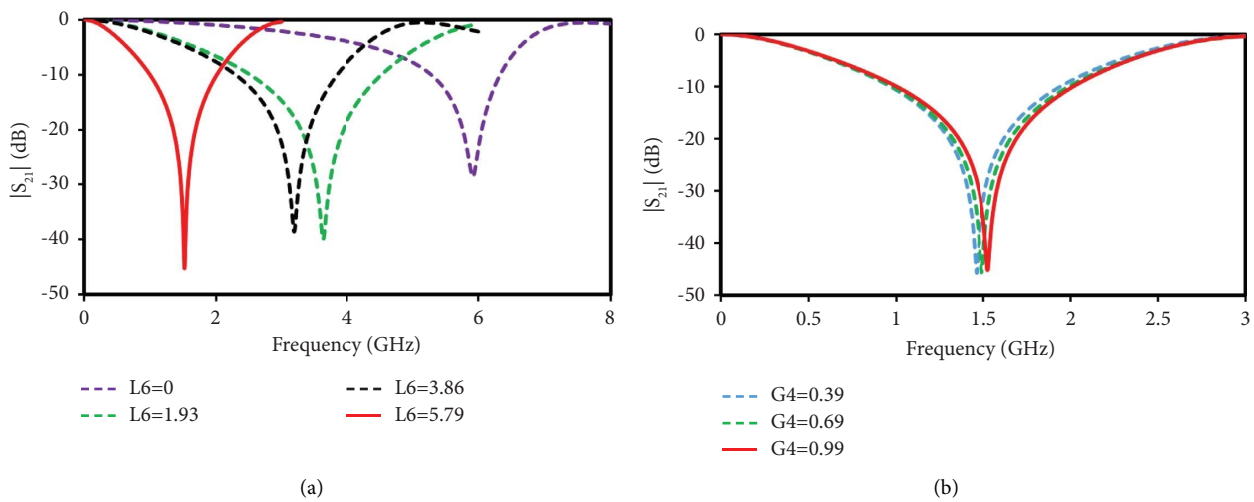

Figure 6: Parametric analysis by varying the parameters of the resonator. (a) Length (L6). (b) Width (G4).

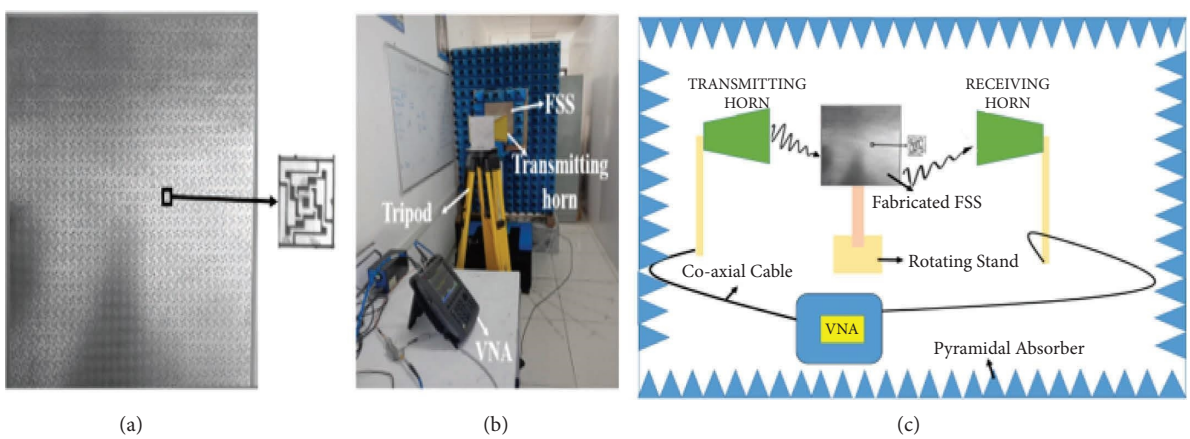

Figure 7: (a) Top layer of the fabricated FSS unit cell. (b) Measurement setup. (c) Schematic diagram of the measurement setup.

3. Measurement and Validation

The fabricated prototype and measurement setup of the FSS unit cell containing the top layer are shown in Figures 7(a) and 7(b), respectively. The schematic diagram of the measurement setup is depicted in Figure 7(c). The fabricated FSS accommodates a 30×30 lattice array containing 900 elements. The unit cell miniaturization helps to achieve a smaller footprint of 270 mm × 270 mm. The horn antenna helps for transmitting and receiving the incident signals where the FSS is placed by a distance of 2 m. Measurement is carried out in an anechoic chamber to avoid signal reflections. The antennas are connected to a two-port vector network analyzer (N9951A). A rotating shaft helps to rotate the FSS for measuring the transmission coefficient at different angles of theta for the incident EM waves. To measure the polarization-independent performance for different angles of phi, the FSS is placed at 0° to measure the $|S_{21}|$ in horizontal polarization (TM Mode) and rotated 90° to obtain the transmission coefficient in vertical polarization (TE Mode). It is inferred from Figure 8 that the proposed single-layer FSS provides the band-stop response from 1 GHz to 2 GHz. Due to the miniaturization of the FSS, the transmission properties become stable leading to less susceptibility to various incidence angles. Shielding effectiveness is related to the S-parameters and it is defined as the inverse of the transmission coefficient denoted by the expression [18] as $\mathrm{SE}\,(\mathrm{dB}) = -|S_{21}|$. It is evident from Figures9(a) and 9(b) that the proposed FSS unit cell offers shielding effectiveness with a peak value of 45.4 dB at a 10 dB reference level for various incidence angles up to 80° in both TE and TM Mode. At a higher angle of oblique incidence, the array elements in the FSS unit cell experience a phase delay in the excitation. This phase difference causes a shift in the operating frequency of the FSS at oblique incidence, which can be reduced by using a small FSS unit cell size. The FSS unit cell periodicity also limits the occurrence of grating lobes. In this paper, a convolution technique is used to attain the ultra-miniaturized geometry with unit cell periodicity of 8.4 mm × 8.4 mm. The ultraminiaturized configuration of the FSS exhibits a stable response at the high oblique incidence of 80° without any frequency shift. Thus, the proposed FSS exhibits

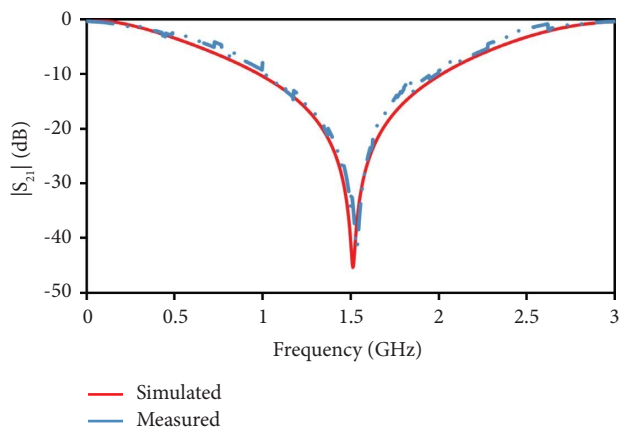

Figure 8: Simulated and measured transmission coefficient characteristics.

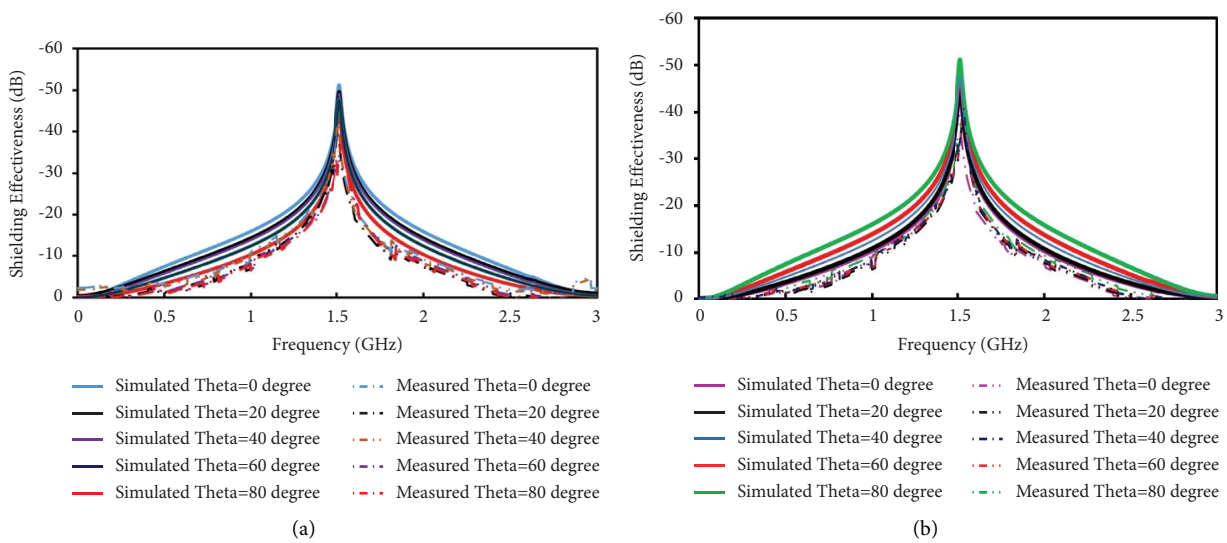

Figure 9: Comparison of simulated and measured SE for various angles of theta. (a) TE mode. (b) TM mode.

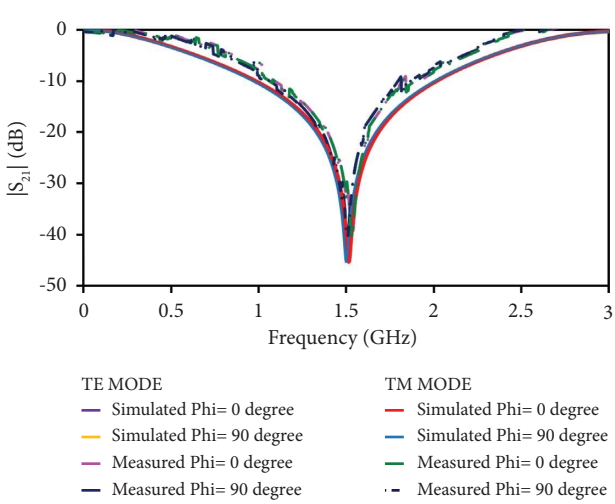

Figure 10: Comparison of simulated and measured $|S_{21}|$ in perpendicular polarization (TM mode) and parallel polarization (TE mode).

high angular stability performance without any frequency shift. Due to the four-fold symmetric nature of the proposed FSS unit cell, the measured result in Figure 10 is polarization independent for the various angles of phi from 0° to 90° in both TE and TM Modes. Table 1 tabulates the similar existing work with the proposed FSS. The miniaturized FSS unit cell with a profile of $0.028\lambda o \times 0.028\lambda o$ is proposed on the single layer of FR-4 substrate to achieve the band-stop response for the entire L-band ranging from 1 to 2 GHz without incorporating conductive holes, thus making lesser fabrication costs when compared with the existing work.

3.1. Performance Comparison. The FSS unit cell comprising a square loop with folded arms acts as a spatial filter for the entire L-band with a miniaturized footprint of $0.028\lambda o$. The proposed FSS unit cell is 88.61%,53.33%,31.21%, 32.1%, 32.18%, and 80.25% smaller when compared to existing art of works [7, 9, 10, 15–17], respectively. The proposed FSS

Table 1: Comparison of the proposed FSS with similar research works.

Ref	Unit cell size	Operating frequency (GHz)	Bandwidth (−10 dB)	Angular stability (°)	Limitations
[7]	$0.083\lambda o \times 0.083\lambda o$	2	1 GHz	60	Higher profile of the FSS unit cell
[10]	$0.041\lambda o \times 0.041\lambda o$	2.47	0.988 GHz	60	Miniaturization is attained for higher operating frequency
[9]	$0.034\lambda o \times 0.034\lambda o$	1.056	0.1 GHz	75	Usage of fractal elements with PTH
[15]	$0.034\lambda o \times 0.034\lambda o$	1.6	0.34 GHz	60	Conductive holes are used
[16]	$0.18\lambda o \times 0.18\lambda o$ (with vias)	0.9 1.9	0.54 GHz, 0.43 GHz	70	Polarization-sensitive due to asymmetric geometry
[17]	$0.063\lambda o \times 0.063\lambda o$	1.9	1.18 GHz	60	Low angular stability
This work	$0.028\lambda o \times 0.028\lambda o$ (without vias)	1-2	1 GHz	80	—

unit cell utilizes only the top layer of the substrate while eliminating the usage of multiple layers as in [8] to avoid a bulkier profile of the FSS. The proposed FSS achieves a miniaturized configuration without using complex conductive holes providing a cost-effective solution, whereas the work in [9, 12, 13] makes use of 2.5D geometry which increases the fabrication costs. The proposed FSS unit cell has a higher shielding effectiveness of 45.4 dB for various angles of theta in both TE and TM modes, whereas the literature reported in [7, 9] shows the lesser effect of eliminating the incoming electromagnetic signals in the desired operating frequency. The proposed FSS has a stable transmission coefficient for various angles of phi from 0° to 90° in both horizontal (TM mode) and vertical polarization (TE Mode) of the EM waves due to its four-fold symmetrical geometry. The FSS in [16] shows polarization insensitivity due to the asymmetric structure. The proposed FSS exhibits angular stability from 0° to 80° under TE and TM mode with a minimum frequency deviation of less than 1% because of its miniaturized footprint unlike in [7, 9, 10, 16, 17]. The depicted FSS unit cell has a larger bandwidth of 1 GHz. However, the existing works in [9, 10, 16] achieve lower bandwidth for the discrete resonating frequency.

4. Conclusion

A single-layer miniaturized FSS unit cell for L-band applications is discussed in this paper. The miniaturized profile of the proposed FSS unit cell is $0.028\lambda o \times 0.028\lambda o$ which achieves the band-stop response from 1 to 2 GHz with a peak shielding effectiveness of 45.4 dB. The proposed FSS unit cell provides the invariant polarization performance and angular stability for various angles of phi and theta up to 90° and 80°, respectively, under TE and TM Mode. The FSS unit cell achieves a fractional bandwidth of 66.67% for L-band frequency ranges from 1 to 2 GHz. The measured results are compared with the simulated results to analyze the performance of the FSS unit cell.

Data Availability

The data used in this study are available from the corresponding author upon request.

Conflicts of Interest

The authors declare that they have no conflicts of interest.

Acknowledgments

This work is supported by Savitribai Jyotirao Phule Fellowship for Single Girl Child instituted by University Grants Commission (UGC) of India.

References

[1] A. Munk, *Frequency Selective Surfaces: Theory and Design*, Wiley, New York, NY, USA, 2000.

[2] Y. Ranga, L. Matekovits, K. P. Esselle, and A. R. Weily, "Multioctave frequency selective surface reflector for ultra-wideband antennas," *IEEE Antennas and Wireless Propagation Letters*, vol. 10, pp. 219–222, 2011.

[3] A. Chatterjee and S. K. Parui, "Performance enhancement of a dual-band monopole antenna by using a frequency-selective surface-based corner reflector," *IEEE Transactions on Antennas and Propagation*, vol. 64, no. 6, pp. 2165–2171, 2016.

[4] F. Bayatpur and K. Sarabandi, "Miniaturized FSS and patch antenna array coupling for angle-independent, high-order spatial filtering," *IEEE Microwave and Wireless Components Letters*, vol. 20, no. 2, pp. 79–81, 2010.

[5] C. Chiu, C. Kuo, and M. Lin, "Bandpass shielding enclosure design using multipole-slot arrays for modern portable digital devices," *IEEE Transactions on Electromagnetic Compatibility*, vol. 50, no. 4, pp. 895–904, 2008.

[6] R. Sivasamy, B. Moorthy, M. Kanagasabai, V. R. Samsingh, and M. G. N. Alsath, "A wideband frequency tunable FSS for electromagnetic shielding applications," *IEEE Transactions on Electromagnetic Compatibility*, vol. 60, no. 1, pp. 280–283, 2018.

[7] A. Dewani, S. G. O'Keefe, D. V. Thiel, and A. Galehdar, "Window RF shielding film using printed FSS," *IEEE Transactions on Antennas and Propagation*, vol. 66, no. 2, pp. 790–796, 2018.

[8] B. Ashvanth, B. Partibane, and M. G. N. Alsath, "An ultra-miniaturized frequency selective surface with angular and polarization stability," *IEEE Antennas and Wireless Propagation Letters*, vol. 21, no. 1, pp. 114–118, 2022.

[9] L. Murugasamy and R. Sivasamy, "A novel fractal inspired iterated four-legged loaded loop elements based 2.5-D miniaturized frequency selective surface," *IEEE Transactions on Electromagnetic Compatibility*, vol. 63, no. 6, pp. 2164–2167, 2021.

[10] S. Khajevandi, H. Oraizi, A. Amini, and M. Poordaraee, "Design of miniaturised-element FSS based on 2.5-dimensional closed loop Hilbert fractal," *IET Microwaves, Antennas & Propagation*, vol. 13, no. 6, pp. 742–747, 2019.

[11] Y.-M. Yu, C.-N. Chiu, Y.-P. Chiou, and T.-L. Wu, "An effective via based frequency adjustment and minimization methodology for single- layered frequency-selective surfaces," *IEEE Transactions on Antennas and Propagation*, vol. 63, no. 4, pp. 1641–1649, 2015.

[12] M. W. Niaz, Y. Yin, and J. Chen, "Synthesis of ultraminiaturized frequency-selective surfaces utilizing 2.5-D tapered meandering lines," *IEEE Antennas and Wireless Propagation Letters*, vol. 19, no. 1, pp. 163–167, 2020.

[13] M. W. Niaz, Y. Yin, S. Zheng, L. Zhao, and J. Chen, "Design and analysis of an ultraminiaturized FSS using 2.5-D convoluted square spirals," *IEEE Transactions on Antennas and Propagation*, vol. 68, no. 4, pp. 2919–2925, 2020.

[14] T. Li, D. Li, P. Qin et al., "A novel miniaturized strong-coupled FSS structure with excellent angular stability," *IEEE Transactions on Electromagnetic Compatibility*, vol. 63, no. 1, pp. 38–45, 2021.

[15] S. S. Sampath, R. Sivasamy, and K. J. J. Kumar, "A novel miniaturized polarization independent band-stop frequency selective surface," *IEEE Transactions on Electromagnetic Compatibility*, vol. 61, no. 5, pp. 1678–1681, 2019.

[16] Y. Ma, W. Wu, Y. Yuan, X. Zhang, and N. Yuan, "A convoluted structure for miniaturized dual-bandstop frequency selective surface," *IEEE Antennas and Wireless Propagation Letters*, vol. 18, no. 2, pp. 328–332, 2019.

[17] H. Li, F. Costa, J. Fang et al., "2.5-D miniaturized multi-functional active frequency-selective surface," *IEEE Transactions on Antennas and Propagation*, vol. 67, no. 7, pp. 4659–4667, 2019.

[18] M. Li, M. Li, Bin, and J. Wei, "A dual-frequency miniaturized frequency selective surface structure suitable for antenna stealth," *Wireless Communications and Mobile Computing*, vol. 2021, Article ID 2861146, 7 pages, 2021.

[19] R. Sivasamy and M. Kanagasabai, "Novel reconfigurable 3-D frequency selective surface," *IEEE Transactions on Components, Packaging, and Manufacturing Technology*, vol. 7, no. 10, pp. 1678–1682, 2017.

[20] J. Volakis, *Antenna Engineering Handbook*, McGraw-Hill, New York, NY, USA, 4th edition, 2007.

[21] A. Kapoor, R. Mishra, and P. Kumar, "Frequency selective surfaces as spatial filters: fundamentals, analysis and applications," *Alexandria Engineering Journal*, vol. 61, no. 6, pp. 4263–4293, 2022.

[22] R. S. Anwar, L. Mao, and H. Ning, "Frequency selective surfaces: a review," *Applied Sciences*, vol. 8, no. 9, p. 1689, 2018.

[23] R. Sivasamy, B. Moorthy, M. Kanagasabai, J. George, L. Lawrance, and D. &Rajendran, "Polarization-independent single-layer ultra-wideband frequency-selective surface," *International Journal of Microwave and Wireless Technologies*, vol. 9, no. 1, pp. 93–97, 2017.

[24] J. KizhekkePakkathillam, M. Kanagasabai, C. Varadhan, and P. Sakthivel, "A novel fractal antenna for UHF near-field RFID readers," *IEEE Antennas and Wireless Propagation Letters*, vol. 12, pp. 1141–1144, 2013.

[25] A. Kapoor, P. Kumar, and R. Mishra, "Modelling of wideband concentric ring frequency selective surface for Gevices," *Computers, Materials & Continua*, vol. 74, no. 1, pp. 341–361, 2023.

[26] W. Afzal, A. Ebrahimi, M. R. Robel, and W. S. T. Rowe, "Low-profile higher-order narrowband bandpass miniaturized-element frequency-selective surface," *IEEE Transactions on Antennas and Propagation*, vol. 71, no. 4, pp. 3736–3740, 2023.

[27] N. Naseer, D. Gokcen, and B. Saka, "Analysis and design of stopband FSS unit cell on textile substrates," *IEEE Letters on Electromagnetic Compatibility Practice and Applications*, vol. 3, no. 1, pp. 15–18, 2021.

[28] J. Ghosh, R. Dutta, A. Sarkhel, and Q. H. Abbasi, "Design of miniaturize flexible wideband frequency selective surface for electromagnetic shielding application," *Waves in Random and Complex Media*, vol. 36, 2022.